INTERNATIONAL JOURNAL OF COMMUNICATION SYSTEMS
Int. J. Commun. Syst. (2014)
Published online in Wiley Online Library (wileyonlinelibrary.com). DOI: 10.1002/dac.2851

Analysis of accessing to the nearest and to the strongest base station in femtocell networks

Huanle Zhang[1], Jian Liu[2,*,†] and Haili Shi[2]

[1] *University of Electronic Science and Technology of China, Chengdu 611731, China*
[2] *University of Science and Technology Beijing, Beijing 10083, China*

SUMMARY

The deployment of femtocells can effectively improve the capacity of cellular networks without significant increase in the network management costs. Femtocell base stations are usually installed by users, which poses unique challenges for future mobile communication standards. The randomness of the locations of femtocells brings us many difficulties to analyze and compare. In this paper, we explore the performance on two different access methods under Rayleigh fading channel: accessing to the nearest and accessing to the strongest femtocell base station. Two performance indexes are of most interest in this paper: how the different path loss exponents and femtocell densities affect the difference of performance between the two different access methods. In the first part of this paper, the distributions of received strength for both access methods are achieved, in which we elaborate the characteristics of received signal strength including the cumulative distribution and the median signal strength. In the second part, we explore the characteristic of SINR distribution, which can be interpreted as the probability of coverage. This paper provides detailed illustrations about how performance changes for these two different access methods under Rayleigh fading channel. All results are mathematically tractable. Copyright © 2014 John Wiley & Sons, Ltd.

Received 25 March 2014; Revised 7 July 2014; Accepted 4 August 2014

KEY WORDS: femtocell; nearest access; strongest access; stochastic geometry; strength loss; SINR distribution

1. INTRODUCTION

Femtocell access points (FAPs), also called 'home base stations', are crucial for next generation cellular networks. Femtocells can effectively improve the capacity of cellular networks without significant increase in the network management costs [1, 2]. FAPs are usually installed by users and deployed in indoor environment. These low-power base stations provide a limited coverage area and connect to the operators' core networks through digital subscriber line, cable broadband connection, or even wireless links [3].

The interest in femtocells in the mobile operator community continues to grow, and according to the Small Cell Forum's reports, the commercial deployments have increased to 41 in 23 countries during 2012. It is estimated by Informa Telecoms & Media that the deployments of small cell market would reach 91.9 million by 2016, with femtocells accounting for more than 80%. It is expected that FAPs would be widely deployed in the near future. Although femtocells can offload traffic from the macro stations and are crucial for next generation mobile communications, special challenges exist because of the randomness of their locations [4–6].

The randomness of the locations of femtocells brings us many difficulties to analyze and compare. Currently, there are three main site modeling methods in femtocell networks: Monte Carlo multicell

*Correspondence to: Jian Liu, School of Computer and Communication Engineering (SCCE), USTB, Beijing 10083, China.
[†]E-mail: liujian@ustb.edu.cn

Copyright © 2014 John Wiley & Sons, Ltd.

model (simulation), signal-cell linear model (deterministic), and stochastic geometry model (statistical) [7]. In order to quantitatively analyze the performance of femtocells, stochastic geometry has been used in some papers. In [8], the authors regard stochastic geometry as one of the four effective tools to solve small cell problems (other three are large random matrix theory, Game theory, and interference alignment and VFDM). The authors in [9] propose a tractable approach to solve the problem of SINR distribution for femtocell networks using stochastic geometry, while in [10], fractional frequency reuse for OFDMA cellular networks is solved. These works are based on homogeneous Poisson point process to model the locations of FAPs. One advantage of using stochastic geometry is the ability to capture the non-uniform layout of modern cellular deployments due to topographic, demographic, or economic reasons [11]. Additionally, tractable expressions can be drawn from the Poisson model, leading to more general performance characterizations and intuition [12].

In this paper, we focus on the performance of two different access methods under Rayleigh fading channel—accessing to the nearest FAP and accessing to the strongest FAP. The nearest access method means that users access to the FAP that is geographically nearest, whereas the strongest access method means that users access to the FAP from which the received signal strength is maximal. Because FAPs will mostly be installed by non-expert users, we expect that these two different access method would result in much different characteristics. Two variables are investigated: how the different path loss exponents and how the femtocell densities affect the performance of these two different access methods.

In the first part of this paper, the distributions of received strength for both methods are studied. Specifically, the cumulative distribution of received signal strength is explored, and how the femtocell density affects the overall performance is also studied. Median signal strength received by users will also be illustrated. In the second part, we explore the characteristics of SINR distributions for both access methods. The SINR distribution can also be interpreted as the probability of coverage, which is a crucial parameter for realistic mobile communications and femtocell deployments.

The contribution of this paper is the systematical analysis on the nearest access method and the strongest access method in femtocell networks under Rayleigh fading channel. In this paper, we offer detailed insight at the performance of these two access methods. Based on stochastic geometry, all the results are tractable.

2. SYSTEM MODEL

In this section, our system model is explained and relevant assumptions are clarified. The main focus of this section is on Poisson point process, which is used to model the locations of FAPs in this paper. The definition of Poisson point process is given in what follows.

Definition 1
Let Λ be a locally finite non-null measure on $\mathbb{R}^d$. The Poisson point process Φ of intensity measure Λ is defined by means of its finite-dimensional distributions:

$$P\{\Phi(A_1) = n_1, ..., \Phi(A_k) = n_k\} = \prod_{i=1}^{k} \left(e^{-\Lambda(A_i)} \frac{\Lambda\left(A_i^{n_i}\right)}{n_i!} \right), \tag{1}$$

for every $k = 1, 2, ...$ and all bounded, mutually disjoint sets A_i for $i = 1, ..., k$. If $\Lambda(dx) = \lambda dx$ is a multiple of Lebesgue measure (volume) in $\mathbb{R}^d$, then Φ is a homogeneous Poisson point process and λ is the intensity.

The realization of Poisson point process (p.p.) can be constructed as follows. If the region considered has an area of $|A|$, then the mean number of points in this region is $\lambda \cdot |A|$. The homogeneous Poisson p.p. can be simply generated by a random variable X following Poisson distribution with parameter $\lambda \cdot |A|$, and each point is distributed uniformly among the region. Figure 1 shows a snapshot from a homogeneous Poisson point process with intensity equal to $200/(500 \times 500)$. As shown

Copyright © 2014 John Wiley & Sons, Ltd.

DOI: 10.1002/dac

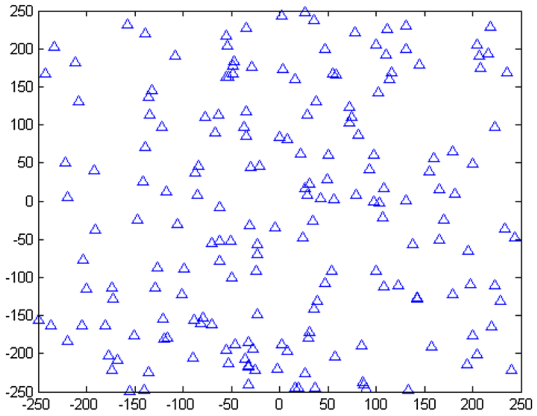

Figure 1. A snapshot of locations of femtocell access points taken from a homogeneous Poisson point process with intensity $200/(500 \times 500)$.

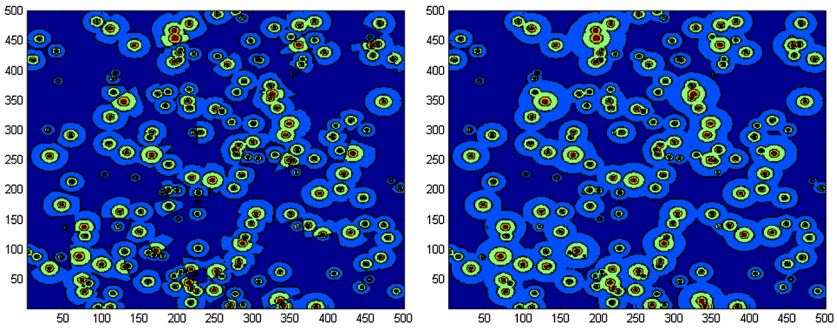

(a) Nearest Case. (b) Strongest Case.

Figure 2. Distribution of received signal strength. Locations of femtocell access points are the same with Figure 1 (coordinates have transformed from -250 to 0).

in Figure 1, the locations of points seem to be stochastic, but it would resemble the locations of FAPs in the near future.

In this paper, locations of FAPs are assumed to follow homogeneous Poisson point process with intensity λ. The effect of macro base station is ignored. The focus of this paper is on femtocell layer, that is, users only access to FAPs. A particular snapshot of homogeneous Poisson point process (Figure 1) is used to help to intuitively present the difference, but please note that our system model is totally following homogeneous Poisson p.p., and all results are derived from rigorous mathematical derivation, which do not depend on one particular locations of FAPs. Two access methods are explored: users access to the nearest FAP and users access to the strongest FAP. The standard power loss propagation model is used with path loss exponent α. As far as random channel effects, we assume that all femtocell base stations and tagged user experience only Rayleigh fading with mean 1, and employ a constant transmit power of $1/\mu$. Thus, the received power of a typical node at a distance r from its FAP is $hr^{-\alpha}$ where the random variable h follows an exponential distribution with mean $1/\mu$, which we denote as $h \sim exp(\mu)$.

3. DISTRIBUTION OF SIGNAL STRENGTH RECEIVED

In this section, the distributions of signal received for both access methods will be studied. The deployment of future FAPs is much probably confirmed to random deployment, so the homogeneous Poisson point process is applied.

In Figure 2, a snapshot of received signal strength is given (the locations of FAPs is shown in Figure 1). It is a snapshot from a homogeneous Poisson point process with mean number of 200

Copyright © 2014 John Wiley & Sons, Ltd.

DOI: 10.1002/dac

FAPs in a region of 500×500 m^2. In fact, the number of FAPs in this snapshot is 188. The red areas are the areas where the loss of received signal strength is less than 10 dB; the orange areas are the areas whose loss are less than 20 dB but larger than 10 dB; the green areas are less than 30 dB but larger than 20 dB; the light blue areas are less than 40 dB but larger than 30 dB, and the dark blue areas are the areas where the loss are larger than 40 dB. Figure 2(a) shows the case when users access to the nearest FAP, while Figure 2(b) shows the case when users access to the strongest FAP. The path loss exponent α is 3 in this snapshot.

It is obvious from Figure 2(a) that in the nearest access method, the areas tend to abrupt while they are very smooth in the strongest access method. In the nearest access method, we can see that the received signal strength will change dramatically, so users would endure terrible experience, whereas in the strongest access method, the change of signal strength is smooth and hence will not result in terrible user experience. Even the coverage area for each case is slightly different and the strongest case shows a better received signal strength. Table I shows the percentage of different coverage areas. This particular locations of FAPs as shown in Figure 1 are used to help intuitively illustrate the performance. However, our system model is homogeneous Poisson point process, and all results are based on rigid mathematical reasoning.

3.1. Mathematical reasoning of signal strength in nearest access method

In this part, performance analysis on received signal strength in the nearest access method will be given. An important quantity is the distance r separating a typical user from its tagged closest FAP. Because each user communicates with his closest FAP in this case, no other base station can be closer than r. The probability density function of r can be derived using the simple fact that the null probability of a 2-D Poisson point process in an area A is $exp(-\lambda \cdot A)$. Hence, we have

$$P\{r > R\} = P\{\text{No FAP closer than R}\} = e^{-\lambda \pi R^2}. \tag{2}$$

Therefore, the cumulative distribution function is $F_r(R) = P\{r \leqslant R\} = 1 - e^{-\lambda \pi R^2}$ and the probability density function can be found as

$$f_r(r) = \frac{\mathrm{d}F_r(r)}{\mathrm{d}r} = 2\pi\lambda r e^{-\lambda \pi r^2}. \tag{3}$$

The subscript r of $f_r(r)$ is a random variable, and the r in parenthesis is a specific instance of the variable. Let $X_{near}(\cdot)$ denote the signal received and for any point $y \in \mathbb{R}^d$, then

$$P\{X_{near}(y) > t \mid r\} = P\{h \cdot r^{-\alpha} > t \mid r\} = P\{h > t \cdot r^{\alpha} \mid r\} = e^{-\mu t r^{\alpha}}, \tag{4}$$

where we have used the fact that for exponential random variable h with parameter μ, $P\{h > s\} = e^{-\mu s}$. If we take mean of r, then (4) turns into

$$\begin{aligned} P\{X_{near}(y) > t\} &= \mathbb{E}_r[P\{X_{near}(y) > t \mid r\}] = \int_0^{\infty} P\{X_{near}(y) > t \mid r\} \cdot f_r(r) dr \\ &= \pi\lambda \cdot \int_0^{\infty} e^{-\mu t r^{\alpha/2}} \cdot e^{-\lambda \pi r} dr, \end{aligned} \tag{5}$$

Table I. Coverage percentage of different losses in each access method.

	Nearest access method Coverage percentage (%)	Strongest access method Coverage percentage (%)
Loss $<$ 10 dB	0.93	0.93
10 dB $\leqslant$ Loss $<$ 20 dB	3.29	3.36
20 dB $\leqslant$ Loss $<$ 30 dB	13.07	13.88
30 dB $\leqslant$ Loss $<$ 40 dB	35.64	41.27
Loss $\geqslant$ 40 dB	47.06	40.56

Copyright © 2014 John Wiley & Sons, Ltd.

DOI: 10.1002/dac

and the cumulative distribution function is

$$F_{near}(t) = P\{X_{near}(y) \leqslant t\} = 1 - P\{X_{near}(y) > t\} = 1 - \pi\lambda \cdot \int_0^\infty e^{-\mu t r^{\alpha/2}} \cdot e^{-\lambda \pi r} dr. \quad (6)$$

Equation (6) characterizes the distribution of received signal strength in the nearest access method. In addition to the distribution of signal strength, the mean signal received is of much interest. However, it is clear that the mean strength received is infinite from the observation that $hr^{-\alpha}$ is infinite as $r \to 0$. Other than considering mean signal strength received, we turn to medium signal strength that is received. Median signal strength means that the received signal for the tagged user is statistically better than half of other users' received signal but worse than the other half. Let $T_{near}(\mu, \alpha)$ denote the medium signal strength, then

$$T_{near}(\mu, \alpha) = \{t : F_{near}(t) = 0.5\}. \quad (7)$$

3.2. Mathematical reasoning of signal strength in the strongest access method

We have achieved the equations for the performance on received signal strength in the nearest access method. In comparison, performance in the strongest case will be explored in this part. Theorem 1 is given first to help us obtain the signal strength in the strongest access method.

Theorem 1
Given a marked point process $\tilde{\Phi}$ and response function $L(y, x, m)$, the extremal shot-noise filed is defined by

$$X_{\tilde{\Phi}}(y) = \sup_{(x_i, m_i) \in \tilde{\Phi}} L(y, x_i, m_i), \quad y \in \mathbb{R}^d, \quad (8)$$

and if that $\tilde{\Phi}$ is an independently marked Poisson p.p. with intensity measure Λ and mark distribution $F_x(dm)$, then

$$P\{X(y) \leqslant t\} = \exp\left\{-\int_{\mathbb{R}^d} \int_{\mathbb{R}^l} \mathbb{1}(L(y, x, m) > t) F_x(dm) \Lambda(dx)\right\}. \quad (9)$$

Proof
According to the Displacement Theorem [13], an independently marked Poisson p.p. $\tilde{\Phi}$ with intensity measure Λ on $\mathbb{R}^d$ and marks with distribution $F_x(dm)$ on $\mathbb{R}^l$ is a Poisson p.p. on $\mathbb{R}^d \times \mathbb{R}^l$ with intensity measure

$$\tilde{\Lambda}(A \times K) = \int_A \tilde{p}(x, K) \Lambda(dx), \quad A \subset \mathbb{R}^d, \ K \subset \mathbb{R}^l, \quad (10)$$

where $\tilde{p}(x, K) = \int_K F_x(dm)$. Consequently, its Laplace transform is equal to

$$\mathscr{L}_{\tilde{\Phi}} = \mathbb{E}\left[\exp\left\{-\sum_i \tilde{f}(x_i, m_i)\right\}\right] = \exp\left\{-\int_{\mathbb{R}^d} \left(1 - \int_{\mathbb{R}^l} e^{-\tilde{f}(x,m)} F_x(dm)\right) \Lambda(dx)\right\}, \quad (11)$$

for all functions $\tilde{f} : \mathbb{R}^{d+l} \to \mathbb{R}^+$. On the other hand,

$$\begin{aligned} P\{X_{\tilde{\Phi}}(y) \leqslant t\} &= P\{L(y, x_i, m_i) \leqslant t \text{ for all } (x_i, m_i) \in \tilde{\Phi}\} \\ &= \mathbb{E}\left[\exp\left\{\sum_{(x_i, m_i) \in \tilde{\Phi}} \log\left(\prod_{j=1}^k \mathbb{1}(L(y, x_i, m_i) \leqslant t)\right)\right\}\right]. \end{aligned} \quad (12)$$

Combining the result of $\mathscr{L}_{\tilde{\Phi}}$ proves the theorem. □

Copyright © 2014 John Wiley & Sons, Ltd.

DOI: 10.1002/dac

Theorem 1 can be used to help us to determine the distribution of received signal strength in the strongest access method. The reasoning is similar with the nearest access method and illustrated briefly as what follows. The probability of signal strength received by the tagged user larger than t is

$$P\{L(y,x,m) > t\} = P\{h \cdot r^{-\alpha} > t\} = P\{h > t \cdot r^{\alpha}\} = e^{-\mu t r^{\alpha}}, \tag{13}$$

where we have used the fact that for exponential random variable h with parameter μ, $P\{h > s\} = e^{-\mu s}$. For homogeneous Poisson point process, we have $\int_{\mathbb{R}^d} f(x)\Lambda(dx) = 2\pi\lambda \int_{\mathbb{R}} f(r) r dr$, and for a annulus with radius of r and width of dr, the total number of *1* in this region is $2\pi r \cdot e^{-\mu t r^{\alpha}} dr$. Hence, we can obtain following relationship:

$$F_{stro}(t) = P\{X(y) \leqslant t\} = \exp\left\{-2\pi\lambda \cdot \int_0^{\infty} r \cdot e^{-\mu t r^{\alpha}} dr\right\}. \tag{14}$$

As in the nearest access method, the medium signal strength received by users is denoted by

$$T_{stro}(\mu,\alpha) = \{t : F_{stro}(t) = 0.5\}. \tag{15}$$

3.3. Performance comparisons

In this part, we will compare the performance on the nearest access method and the strongest access method. First, cumulative distributions of received signal strength are compared. Next, how the distributions of received signal strength change with femtocell densities for both methods is given. Finally, median signal strength received by each method will be explored.

3.3.1. Distribution of received signal strength. Because we omit the noise (or the noise could be assumed constant and hence do not affect the performance difference of these two access methods) and each FAP transmits at a fixed and equal power, the value of transmit power is irrelevant. In this part, we explore the loss of signal strength received. Figure 3 shows the cumulative distribution function according to (6) and (14). Three cases are shown: path loss exponent of 2, 3, and 4, which is presented by red, blue, and black lines, respectively. The dashed lines represent the nearest access method, whereas the solid lines represent the strongest access method. The intensity λ is 0.001, corresponding to a region with radius of 250 m; the mean number of FAPs is 200.

It is clear from Figure 3 that the difference between the nearest access method and the strongest access method is more dramatic when the path loss exponent α is small. For example, as can be seen from the figure, the received signal strength is nearly unlikely lower than 30 dB in the strongest access method (2.87%) when the path loss exponent α is 2, whereas in the nearest access method, the probability is as high as 21.97%. In the cases when exponent α equals 4, however, the difference is less obvious and the signal strength received tends to endure attenuation more than 40 dB.

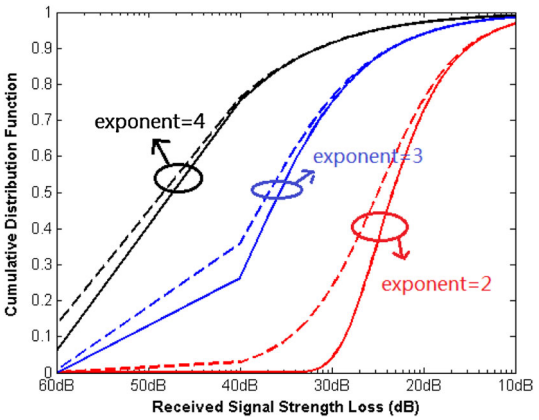

Figure 3. Cumulative distribution for received signal strength loss for both access methods.

Copyright © 2014 John Wiley & Sons, Ltd.

DOI: 10.1002/dac

3.3.2. Probability of signal strength whose loss > 30 dB. In Figure 4, we show how the probability of received signal strength whose loss is larger than 30 dB changes as the femtocell density increases. Three cases are shown: path loss exponent of 2, 3, and 4, which is presented by red, blue, and black lines, respectively. The dashed lines represent the nearest access method, whereas the solid lines represent the strongest access method.Transmit power of each FAP is assumed to be 1. It is obvious from Figure 4 that as the femtocell density increases, the probability of signal strength loss larger than 30 dB decreases, which is in accordance with our intuition. The difference between these two different access methods, however, highly depend on the path loss exponent. The higher the path loss exponent, the less difference we can see.

3.3.3. Median signal strength received. The medium signal strength received can be obtained from the cumulative distribution function. Figure 5 shows the medium signal strength received as femtocell density changes based on (7) and (15) where we assume that transmit power of each FAP is 1. Three cases are shown: path loss exponent of 2, 3, and 4, which is presented by red, blue, and black lines, respectively. The dashed lines represent the nearest access method, whereas the solid lines represent the strongest access method. As can be seen from Figure 5, the medium signal strength received has a close relationship with path loss exponents. An interesting phenomenon is that with the femtocell intensity increasing, the median is increasing linearly. Obviously, the slope of the strongest access method is higher than nearest counterparts.

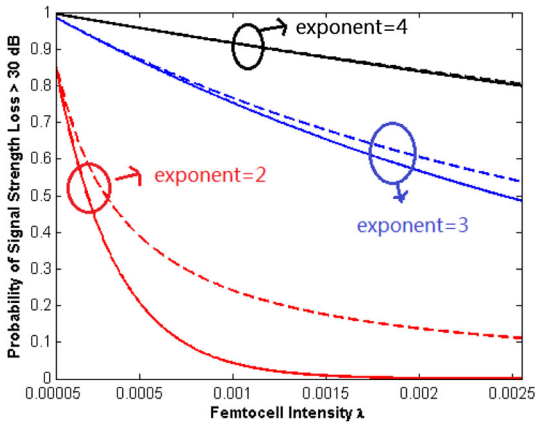

Figure 4. Probability of signal strength whose loss > 30 dB for both access methods.

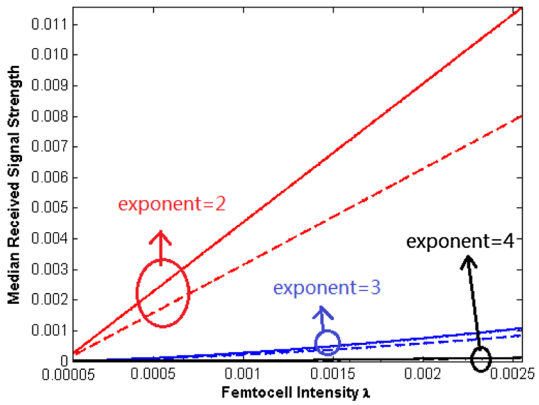

Figure 5. Median received signal strength versus femtocell intensity for both access methods.

Copyright © 2014 John Wiley & Sons, Ltd.

DOI: 10.1002/dac

4. DISTRIBUTION OF SIGNAL-TO-INTERFERENCE-PLUS-NOISE RATIO

In this section, the distribution of SINR experienced by users is explored. Compared with the received signal strength discussed in the previous sections, SINR is of much more interest. The relevant assumptions are the same as have been clarified earlier. Specifically, we ignore frequency reuse such as strict fractional frequency reuse [14, 15] and soft fractional frequency reuse [16, 17], or interference coordination and cancelation techniques [18–20]. Cognitive technique is also one of the effective methods [21].

Intuitively, the SINR for the strongest access method may be slightly higher than the nearest access method. However, the difference is much more dramatic compared to the received signal strength, which we have already discussed. Figure 6 shows the SINR distribution for these two difference access methods (noise is ignored). Figure 6(a) shows the case that users access to the nearest FAP, while Figure 6(b) shows the case that users access to the strongest FAP. The red area in the figure is where the SINR larger than 1; the green area is where the SINR larger than 0.5 but less than 1; the blue area is where the SINR less than 0.5. As can be seen from Figure 6, the blue area (which represents the area of SINR less than 0.5) is much smaller in the strongest access method than in the nearest access method. It is also obvious that the areas tend to be much more smooth in the strongest access method. The distribution of SINR for both access methods will be explored exhaustively in the rest of this section. Once the distribution of SINR has been achieved, other performance can be easily achieved [22, 23], such as the traffic analysis of Skype [24] and VoIP [25].

The proportion of each area in this particular snapshot is presented in Table II. It is outstanding that the percentage of SINR less than 0.5 is much lower in the strongest access method than in the nearest access method, with the reduction reaching 14%.

4.1. *Mathematical reasoning of SINR in nearest access method*

The SINR distribution for the nearest case has already been analyzed in [9]. For comparison, the procedure is quoted here, which can be used to help achieve the performance in the strongest access method.

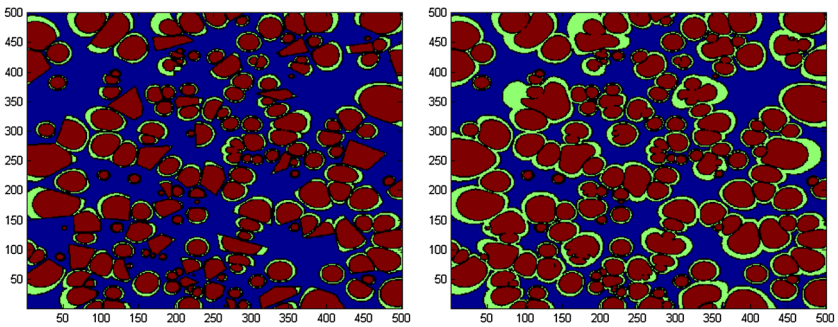

(a) Nearest Case. (b) Strongest Case.

Figure 6. Distribution of SINR for both access methods (noise is ignored). Locations of FAPs are the same with Figure 1 (coordinates have transformed from −250 to 0).

Table II. Percentage of different SINR in each access method.

	Nearest access method Percentage (%)	Strongest access method Percentage (%)
SINR $\geqslant 1$	41.62	46.81
$0.5 \leqslant$ SINR < 1	15.25	24.06
SINR < 0.5	43.13	29.12

Copyright © 2014 John Wiley & Sons, Ltd.

DOI: 10.1002/dac

The SINR of the mobile user at a random distance r from its associated base station can be expressed as

$$\mathrm{SINR} = \frac{hr^{-\alpha}}{I_r + w} \tag{16}$$

where

$$I_r = \sum_{i \in \Phi / b_o} h_i R_i^{-\alpha}, \tag{17}$$

is the cumulative interference from all other FAPs (except the tagged base station for the mobile user at o denoted by b_o), which are at a distance R_i from the typical user and have fading value h_i. W is the noise experienced by the tagged user. Given the distance from the nearest base station, the probability that the SINR of this typical user larger than T is

$$\begin{aligned} P\{SINR > T \mid r\} &= P\left\{\frac{hr^{-\alpha}}{I_r + w} > T \mid r\right\} = P\{h > T \cdot r^{\alpha} \cdot (I_r + w) \mid r\} \\ &= \mathscr{L}_{I_r}(\mu T r^{\alpha}) \cdot \mathscr{L}_{w}(\mu T r^{\alpha}) \end{aligned} \tag{18}$$

in which $\mathscr{L}_{I_r}(s)$ and $\mathscr{L}_{w}(s)$ is the Laplace transform of random variable I_r and w evaluated at s under the condition that the distance to the closest FAP from the origin is r. We will calculate $\mathscr{L}_{I_r}(s)$ in the following (calculation of $\mathscr{L}_{w}(s)$ is similar).

$$\begin{aligned} \mathscr{L}_{I_r}(s) &= \mathbb{E}_{I_r}\left[e^{-s \cdot I_r}\right] = \mathbb{E}\left[\exp\left(-s \cdot \textstyle\sum_{i \in \Phi / b_o} h_i R_i^{-\alpha}\right)\right] \\ &= \exp\left(-2\pi\lambda \cdot \int_r^{\infty} \left[1 - \mathbb{E}_h\left(e^{-s \cdot h \cdot v^{-\alpha}}\right)\right] v dv\right), \end{aligned} \tag{19}$$

where an identity has been used that for Poisson point process, $\mathscr{L}_{\Phi}(f) = \exp\left(-\int_{\mathbb{R}^d}\left(1 - e^{-f(x)}\right)\right.$ $\left.\Lambda(dx)\right)$. Because $h \sim \exp(\mu)$, we have

$$\mathbb{E}_h\left(e^{-s \cdot h \cdot v^{-\alpha}}\right) = \int_0^{\infty} e^{-s \cdot h \cdot v^{-\alpha}} \mu e^{-\mu h} dh = \frac{\mu v^{-\alpha}}{s + \mu v^{\alpha}}, \tag{20}$$

Substituting (20) into (19) comes

$$\mathscr{L}_{I_r}(s) = \exp\left(-2\pi\lambda \cdot \int_r^{\infty} \frac{s \cdot v}{s + \mu v^{\alpha}} dv\right). \tag{21}$$

The same procedure could be used to solve $\mathscr{L}_{w}(s)$. Then, (18) turns into

$$P\{SINR > T \mid r\} = \exp\left(-2\pi\lambda \cdot \int_r^{\infty} \frac{T r^{\alpha} v}{T r^{\alpha} + v^{\alpha}} dv\right) \cdot \mathscr{L}_{w}(\mu T r^{\alpha}). \tag{22}$$

As $P\{SINR > T \mid r\}$ has been achieved, $P\{SINR > T\}$ can easily be obtained from de-conditioning r. If we ignore the effect of noise, which is reasonable because we just compare the difference between those two different access methods, then we have

$$G_{near}(T) = P\{SIsNR > T\} = \mathbb{E}_r[P\{SINR > T \mid r\}] \overset{\text{simplified}}{=\!=\!=} \frac{1}{1 + \beta(T, \alpha)}, \tag{23}$$

where $\beta(T, \alpha) = T^{2/\alpha} \cdot \int_{T^{-2/\alpha}}^{\infty} \frac{1}{1 + u^{\alpha/2}} du$.

Copyright © 2014 John Wiley & Sons, Ltd.

DOI: 10.1002/dac

Equation (23) is the distribution of SINR in the nearest access method. It is worth to note that (23) is unrelated with the femtocell density, which is in accordance with the fact that in an interference-limited network, adding more base stations cannot improve the SINR experienced by users.

4.2. Mathematical reasoning of SINR in strongest access method

The mathematical reasoning of the distribution of SINR in the strongest access method can be aided with the nearest counterpart. Because we have achieved the median signal received in both access methods, $T_{near}(\mu, \alpha)$ and $T_{stro}(\mu, \alpha)$, the effective signal power received in the strongest access method is

$$hr^{-\alpha} \cdot \frac{T_{stro}(\mu, \alpha)}{T_{near}(\mu, \alpha)}, \tag{24}$$

where r is the same as in the nearest access method. The interference experienced by this particular user is

$$I_r - hr^{-\alpha} \cdot \left(\frac{T_{stro}(\mu, \alpha)}{T_{near}(\mu, \alpha)} - 1 \right). \tag{25}$$

As similar as in the nearest access method, the distribution of the SINR (noise is ignored) is

$$\begin{aligned} P\{SINR > T \mid r\} &= P\{h > T' \cdot r^{\alpha} \cdot I_r \mid r\} = \mathbb{E}_{I_r}[P\{h > T' \cdot r^{\alpha} I_r \mid r, I_r\}] \\ &= \mathbb{E}_{I_r}\left[\exp\left(-\mu T' r^{\alpha}\right) \mid r\right] = \mathscr{L}_{I_r}\left(\mu T' r^{\alpha}\right) \end{aligned} \tag{26}$$

where $\mathscr{L}_{I_r}(s)$ is defined in (16) and

$$T' = T \cdot \frac{T_{near}(\mu, \alpha)}{(T+1) \cdot T_{stro}(\mu, \alpha) - T \cdot T_{near}(\mu, \alpha)}. \tag{27}$$

So far, the distributions for both access methods have been achieved. In the rest of this section, the performance will be compared.

4.3. Performance comparisons

For interference-limited mobile networks, the femtocell intensities have no influence on the SINR experienced by users in the nearest access methods. Intuitively, this means that increasing the number of FAPs does not affect the coverage probability, which matches empirical observations in interference-limited urban networks as well as predictions of traditional, less-tractable models. However, this is not true for the strongest access method. In this part, we not only explore the performance differences between the nearest access method and the strongest access method but also show how the femtocell densities affect the performance of the strongest access method. Analysis is based on (23) and (26). Because only when path loss exponent $\alpha > 2$ does the equations for distributions of SINR converge, we only consider the cases for path loss exponents 3 and 4.

Figures 7–9 show the cases when densities of femtocell are very small (intensity of 0.0005), light dense (intensity of 0.0015), and dense (intensity of 0.0025). In all these three figures, blue lines and black lines present the cases when path loss exponent α is 3 and 4, respectively. Dashed lines present the nearest access method, while the solid lines present the strongest cases. The only difference among these three figures are the femtocell densities.

An interesting phenomenon worth noting is that when the deployment of femtocells is light, there is no performance improvement for the strongest access method against the nearest access method when the path loss exponent is 4. It is consistent with the result of Figure 5 (see black lines) in which the median signal strength is almost the same. As the density increases, the improvement is obvious. However, when the femtocell density continues to increase, the gain is almost fixed and no more improvement can be seen. Considering Figures 8 and 9, we can also conclude that no difference can be seen if the deployment density of femtocells transcends a certain value.

Copyright © 2014 John Wiley & Sons, Ltd.

DOI: 10.1002/dac

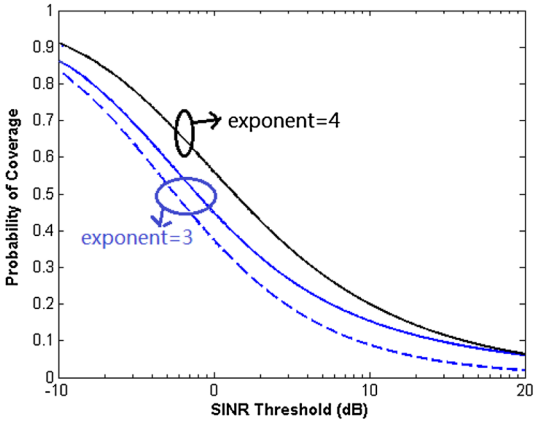

Figure 7. SINR distribution. The femtocell intensity is 0.0005. Lines for $\alpha = 4$ are overlapped.

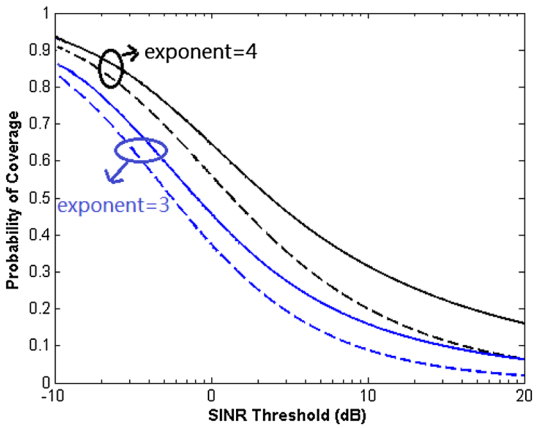

Figure 8. SINR distribution. The femtocell intensity is 0.0015.

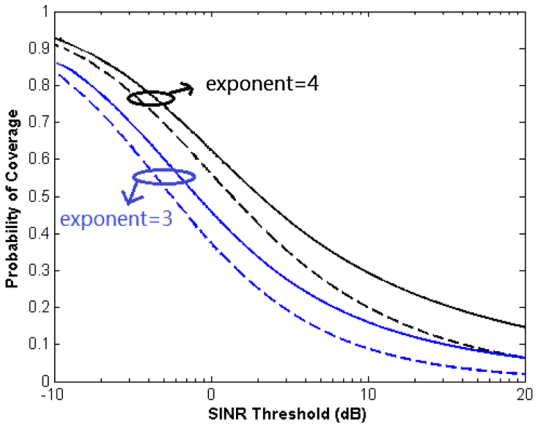

Figure 9. SINR distribution. The femtocell intensity is 0.0025.

5. CONCLUSION

Deployments of femtocells can effectively improve the capacity of cellular networks without significant increase in the network management costs. Femtocell base stations are usually installed by users, which poses unique challenges for future mobile communication standards. The randomness of the locations of femtocells brings us many difficulties to analyze and compare.

Copyright © 2014 John Wiley & Sons, Ltd.

DOI: 10.1002/dac

In this paper, performance on accessing to the nearest and to the strongest femtocell base station under Rayleigh fading is explored. First, the distribution function of received signal strength has been studied. Specifically, the cumulative distribution function and the probability of received signal strength whose loss is lager than 30 dB have been drawn. The factors that influence the performance include path loss exponent and femtocell densities. Especially, different path loss exponents lead to a dramatic difference between these two access methods.

After the studies of signal strength received in both access methods, we turn to SINR, which is of more interest to realistic communication. For interference-limited mobile network, the femtocell density has no influence on the SINR experienced by users in the nearest access method. The probabilities of experienced SINR have been studied exhaustively. We have found that when the deployment of femtocells is light, there is no performance improvement for the strongest access method against the nearest access method in the cases when the path loss exponent is 4. As the density increases, the improvement is obvious. However, when the femtocell density continues to increase, the gain is almost level and no more improvement can be seen.

This paper gives a systematical analysis on two different access methods: accessing to the nearest femtocell base station and accessing to the strongest femtocell base station. Two performance indexes are investigated: the characteristic of received signal strength and the characteristic of experienced SINR. All results are mathematically tractable.

ACKNOWLEDGEMENTS

This work is supported by the National Major Projects (No. 2012ZX03001029-005, 2012ZX03001032-003), National Natural Science Foundation of China (Nos. 60932002, 61173149), and Fundamental Research Funds for the Central Universities (No. FRF-TP-12-080A).

REFERENCES

1. Chandrasekhar V, Andrews JG, Gatherer A. Femtocell networks: a survey. *IEEE Comunication Magazine* 2008; **46**(9):59–67.
2. Claussen H, Ho LTW, Samuel LG. Financial analysis of a pico-cellular home network deployment. *IEEE International Conference on Communications*, Glasgow, 2007; 5604–5609.
3. Claussen H. Performance of macro- and co-channel femtocells in a hierarchical cell structure. *IEEE International Symposium on Personal, Indoor and Mobile Radio Communications*, Athens, 2007; 1–5.
4. Andrews JG, Claussen H, Dohler M, Rangan S, Reed MC. Femtocells: past, present, and future. *IEEE Journal on Selected Areas In Communications* 2012; **30**(3):497–508.
5. Xidong W, Wei Z, Zhaoming L, Xiaoming W, Wei L. Dense femtocell networks power self-optimization: an exact potential game approach. *International Journal of Communication System* 2014. DOI: 10.1002/dac.2788.
6. Chunyan A, Renchao X, Hong J, Yi L. Pricing and power control for energy-efficient radio resource management in cognitive femtocell networks. *International Journal of Communication System* 2013. DOI: 10.1002/dac.2700.
7. Weisi G, Siyi W, Xiaoli C, Jiming C, Hui S. Automated small-cell deployment for heterogenous cellular networks. *IEEE Communications Magazine* 2013; **51**(5):46–53.
8. Hoydis J, Debbah M. Green, cost-effective, flexible, small cell networks. *IEEE Communication Society MMTC* 2010; **5**:23–26.
9. Andrews JG, Baccelli F, Ganti RK. A tractable approach to coverage and rate in cellular networks. *IEEE Transactions on Communications* 2011; **59**(11):3122–3134.
10. Novlan TD, Ganti RK, Ghosh A, Andrews JG. Analytical evaluation of fractional frequency reuse for OFDMA cellular netowrks. *IEEE Transactions on Communications* 2011; **10**(12):4294–4305.
11. Haenggi M, Andrews JG, Baccelli F, Dousse O, Franceschetti M. Stochastic geometry and random graphs for analysis and design of wireless networks. *IEEE Journal on Selected Areas in Communications* 2009; **27**(7):1029–1046.
12. Ganti RK, Baccelli F, Andrews JG. A new way of computing rate in cellular networks. *IEEE International Conference on Communicaitons*, Kyoto, 2011; 1–5.
13. Francois B, Bartlomej B. *Stochastic Geometry and Wireless Networks*. B. NoW Publishers: Paris, 2009. 10–10.
14. Begain K, Rozsa G, Pfening A, Telek M. Performance analysis of GSM networks with intelligent underlay-overlay. *International Symposium on Computers and Communications*, Taormina-Giardini Naxos, 2002; 135–141.
15. Sternad M, Ottosson T, Ahlen A, Svensson A. Attaining both coverage and high spectral efficiency with adaptive OFDM downlinks. *IEEE Vehicular Technology Conference*, Vol. 4, 2003; 2486–2490.
16. Li J, Shroff NB, Chong EKP. A reduced-power channel resue scheme for wireless packet cellular networks. *IEEE/ACM Transactions on Networking* 1999; **7**(6):818–832.
17. Dolppler K, Wijting C, Valkealahti K. Interference aware scheduling for soft frequency reuse. *IEEE Vehicular Technology Conference*, Barcelona, 2009; 1–5.

Copyright © 2014 John Wiley & Sons, Ltd.

18. Rahman M, Yanikomeroglu H, Wong W. Interference avoidance with dynamic inter-cell coordination for downlink LTE system. *IEEE Wireless Communications and Networking Conference*, Budapest, 2009; 1–6.
19. Fodor G, Koutsimanis C, Rácz A, Simonsson NR, Miiller W. Intercell interference coordination in OFDMA networks and in the 3GPP long term evolution system. *Journal of Communications* 2009; **4**(7):445–453.
20. Xiang Y, Luo J, Hartmann C. Inter-cell interference mitigation through flexible resource reuse in OFDMA based communication networks interference coordination in the LTE uplink. *European Wireless Conference*, Paris, 2007; 1–7.
21. Zhong C, Lan-Juan Y, Yong Z, Xian-Da Z. Sensing OFDM systems with timing and frequency offest for cognitive radio networks. *International Journal of Communication System* 2014; **27**(1):184–193.
22. Mogensen P, Na W, Kovacs IZ, Frederiksen F, Pokhariyal A, Pedersen KI, Kolding T, Hugl K, Kuusela M. LTE capacity compared to the Shannon bound. *IEEE Vehicular Technology Conference*, Dublin, 2007; 1234–1238.
23. Teleta E. Capacity of multi-antenna Gaussian channels. *European Transactions on Telecommunications* 1999; **10**(6):585–595.
24. Davide A, Christian C, Stefano G, Michele P, Teresa P. Skype-Hunter: a real-time system for the detection and classification of Skype traffic. *International Journal of Communication System* 2012; **25**(3):386–403.
25. Inoie A. Audio quality in lossy networks for media-specific forward correction schemes. *International Journal of Communication System* 2012; **27**(2):289–302.

Copyright © 2014 John Wiley & Sons, Ltd.

DOI: 10.1002/dac